2023 IEEE/MTT-S International Microwave Symposium - IMS 2023 | 979-8-3503-4764-7/23/$31.00 ©2023 IEEE | DOI: 10.1109/IMS37964.2023.10188011

A Converged Optical and mm-Wave, Dual-band, Multi-beam Rotman Lens Antenna System Enabling Simplified Designs of 5G/mmW Base Stations and Network Densification

Lauryn Smith[#1], Charles Lynch[#2], C. Alex Kaylor[$3], L. Alberto Campos[*4], Lin Cheng[*5], Stephen Ralph[$6], Manos M. Tentzeris[#7]

[#]ATHENA Lab, School of Electrical and Computer Engineering, Georgia Institute of Technology, USA
[$]Georgia Electronic Design Center, School of Electrical and Computer Engineering, Georgia Institute of Technology, USA
[*]CableLabs, USA

[1]lsmith388@gatech.edu, [2]clynch19@gatech.edu, [3]alexkaylor@gatech.edu, [4]a.campos@cablelabs.com, [5]l.cheng@cablelabs.com, [6]stephen.ralph@ece.gatech.edu, [7]etentze@ece.gatech.edu

Abstract — **The current state of the 5G/mmW (mmWave) wireless base stations makes network densification a challenging task. Its complex design, requires a large quantity of complex beam-forming systems, processing components, etc. which when integrating at the system level limits the bandwidth of operation of the beam-forming capabilities. In this effort, a converged optical and mmW system with modulation in the optical domain, simultaneous operation at multiple bands, and multiple beams at-a-time is presented for the simplification of the base station design, through the use of a dual-band Rotman lens antenna system. Error-free over-the-air transmission of 0.930 Gbit/s of total throughput is presented with the proposed dual-band Rotman lens antenna system and a receiver antenna for a proof-of-concept prototype system.**

Keywords — **5G, millimeter-Wave, radio-over-fiber, Rotman lens.**

I. Introduction

Despite the growing interest in 5G/mmW wireless communications, achieving small-cell Ultra Dense Networks (UDNs) is still a major challenge. One significant impediment is the typically high complexity of the base stations. Due to the narrowband nature of commonly used mmW devices, a growingly large number of individual systems are required to support the ever increasing frequency spectrum. Additionally, typical beam forming devices support only one beam at a time. Thus, for example if 7 beams —thereby resulting in seven individual beam-forming devices—are needed for 90° coverage, then the system would require 28 individual devices for 360° coverage at a single frequency band, as well as individual modulating and processing components. Therefore, space and complexity requirements make the implementation and maintenance of 5G/mmW base stations prohibitively expensive. Recently, researchers have been interested in multi-band/wide-band, multi-beam, beam-forming devices, however they typically require three-dimensional structures [1], butler matrices [2], and many array elements to form a few beams.

At mmW frequencies the Rotman lens is a simple, compact, fully-passive, printable, beam-forming device that operates on the principle of true-time delay [3]. This true-time delay property exhibits beam-forming capabilities over a wide bandwidth. The Rotman lens has been implemented in the past [4],[5] in wideband antenna designs taking advantage of the lenses' wideband properties. However, providers usually have licenses in bands covering discrete portions of spectrum, which influences the decision of a simple multi-band design as opposed to a more complex wide-band design. Previously, two Rotman lens antenna systems were combined in an mmID for dual-frequency operation [6], however in this work the dual resonances are supported in a singular Rotman lens antenna structure.

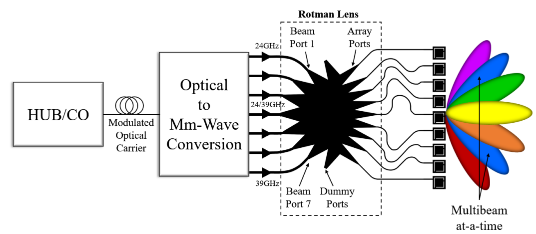

Fig. 1. Schematic of the proposed dual-band (24/39 GHz), optical-to-mmW converged Rotman lens system for 5G/mmW base station simplification.

In Fig. 1, a simplified 5G/mmW base station antenna system is described taking advantage of the broadband nature of optical devices and of the Rotman lens. Taking advantage of the broadband nature of optical devices, the base station can be drastically simplified. Using the existing low-loss fiber network, remote processing at central hubs/central offices (CO) (where real estate, maintenance, and power are inexpensive) enables multi-band processing and reduction of base station complexity. By using a high-speed photodetector at the base station, the signals are converted to the mmW domain while avoiding complex and noisy electrical frequency conversion techniques. A single subsequent dual-band Rotman antenna permits simultaneous communication on multiple frequencies in multiple spatial channels enabling multiple beams.

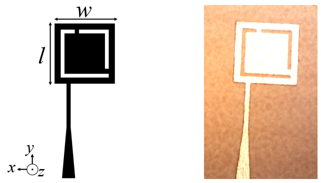

(a) (b)

Fig. 2. Dual-band, slotted patch antenna operating at 24 GHz and 39 GHz (a) schematic, with dimensions l = w = 3 mm and (b) fabricated dual-band patch prototype for measurement validation.

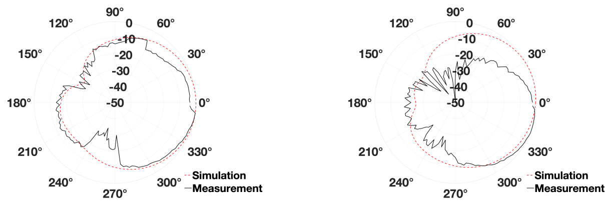

(a) (b)

Fig. 3. Simulated and measured radiation patterns of the dual-band patch antenna at (a) 24 GHz and (b) 39 GHz.

II. Design and Measurement Verification

A. Dual-band Patch Antenna Element

Fig. 2(a) shows the schematic and the dimensions of the proof-of-concept dual-band patch antenna element designed for resonance at 24 GHz and 39 GHz. The substrate material for the design is RO3003 ($\epsilon_r = 3.0$, $tan\delta = 0.009$) with a thickness of $0.25\,\mathrm{mm}$. The patch antenna has an overall size of $3 \times 3\,\mathrm{mm}$, with slot widths of $0.2\,\mathrm{mm}$. The dual-resonance is achieved through genetic algorithm optimization to maximize realized gain at both frequencies of interest, where the variables are the lengths of the outer and inner elements, and the dimensions of the L-shaped slots. The fabricated antenna element is shown in Fig. 2(b). A tapered microstrip line is added to transform the input impedance of the antenna ($90\,\Omega$) to ($50\,\Omega$) for measurement validation using the Vector Network Analyzer.

In simulations the antenna features a $-10\,\mathrm{dB}$ bandwidth of about $800\,\mathrm{MHz}$ at both resonances around $23.8\,\mathrm{GHz}$ and $39.1\,\mathrm{GHz}$. The simulated and measured radiation patterns of the dual-band patch antenna at 24 GHz and 39 GHz are shown in Fig. 3 (a) and (b) demonstrating a good agreement between simulation and measurement results. The antenna is directive in the +z-direction and has a simulated realized gain of $5.4\,\mathrm{dBi}$ at 24 GHz and $5.5\,\mathrm{dBi}$ at 39 GHz.

B. Integrated Dual-band Rotman Lens Antenna Array

The integrated dual-band Rotman lens antenna array shown in Fig. 1 is designed on the same RO3003 substrate material. Since the dual-band patch antennas have input impedance of $90\,\Omega$, the array ports have a longer taper compared to the beam ports ($50\,\Omega$) for matching. An angular coverage of at least 90° is desired, with the aim to implement four Rotman lens antenna systems for a full 360° coverage. Considering the relation between the number of beam ports/array ports combinations and maximum array factor and angular coverage established in [7], simulation of three configurations of beam and array ports (6 beam ports and 8 array ports (6/8), 7 beam ports and 9 array ports (7/9), and 9 beam ports and 12 array ports(9/12)) showed the 7/9 configuration is optimal. The deciding factors taken into account are the number of dummy ports, loss in the dummy ports, array factor, and angular coverage. Although there are trade-offs between the designs, the 7/9 configuration is chosen since the odd number of beam ports provides a middle beam and there are only two dummy ports, thus there is less loss in the dummy ports compared to the 9/12 configuration. The 7/9 configuration also provides the desired angular coverage. Since the Rotman lens design targets two frequencies, 24 GHz and 39 GHz, a parameter study is performed to determine the effect of the array element spacing on the presence of side-lobes. Simulations with array spacing of $\lambda_{24GHz}/2$ (lower resonance), $\lambda_{31.5GHz}/2$ (mean of resonances), and $\lambda_{39GHz}/2$, demonstrate that the latter is ideal to reduce side lobes at 39 GHz.

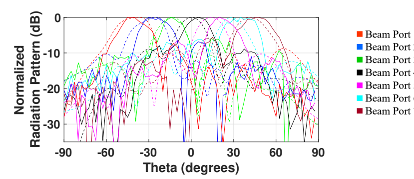

(a)

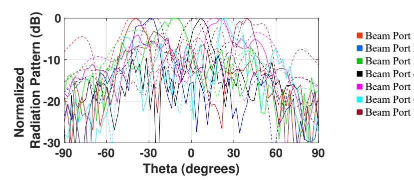

(b)

Fig. 4. Simulated (dashed) and measured (solid) radiation patterns of integrated dual-band Rotman lens antenna at (a) 24 GHz and (b) 39 GHz.

The simulated and measured radiation patterns at (a) 24 GHz and (b) 39 GHz are shown in Fig. 4. The measurement results agree well with simulation and a minor variation in beam location is likely the result of slight misalignments during measurements. The $-3\,\mathrm{dB}$ angular coverage is 100° at 24 GHz and 86 ° at 39 GHz. The simulated realized gains for beam port 1 through 7 (labelled in Fig. 1) at 24 GHz are between $8.2\,\mathrm{dBi}$ and $7.7\,\mathrm{dBi}$, respectively. At 39 GHz, the realized gains are between $10.8\,\mathrm{dBi}$ and $7.8\,\mathrm{dBi}$. The higher gain at 39 GHz is likely a result of the selection of array element spacing of $\lambda_{39GHz}/2$. In future work, the dual-band Rotman lens antenna will be optimized to reduce the presence of side lobes and for a steady gain across the angular bandwidth, particularly by performing a finer parametric study of array factor to determine an optimal trade off.

III. Proof-of-Concept System Demonstration

Fig. 5 depicts a schematic of the measurement setup for proof-of-concept demonstration. First, a Keysight M8196

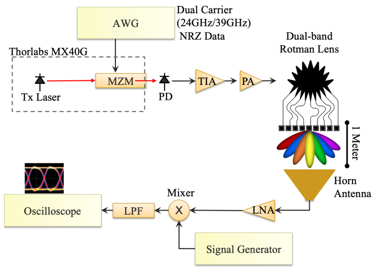

Fig. 5. Schematic of the experimental proof-of-concept dual-band, optical-to-mmW converged Rotman lens system for 5G/mmW base station simplification.

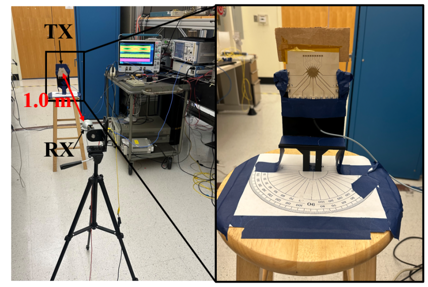

Fig. 6. Measurement set up for the proof-of-concept dual-band, optical-to-mmW converged Rotman lens system demonstration.

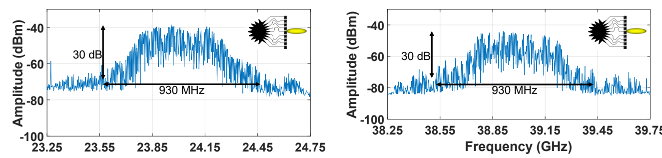

(a) (b)

Fig. 7. Signal Spectrum for optically feeding Beam Port 4 of the dual-band Rotman lens at (a) 24 GHz and (b) 39 GHz.

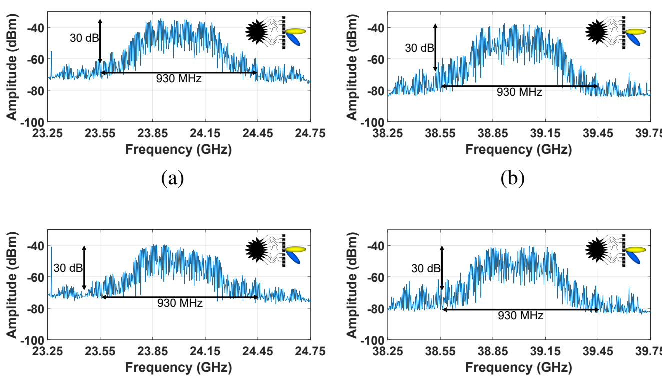

(c) (d)

Fig. 8. Signal Spectrum for optically feeding beam port 4 and beam port 6 of the dual-band Rotman lens to demonstrate multi-beam at a time interrogating at first beam peak (0°) at (b) 24 GHz and (b) 39 GHz and interrogating at the second beam peak (30°) at the (c) 24 GHz and (d) 39 GHz.

Arbitrary Waveform Generator (AWG) is used to generate two electrical signals at 24 GHz and 39 GHz, modulated with 465 MBaud BPSK signals. The system employs raised cosine pulse shaping and encodes using the psedorandom binary sequence PRBS7. The output of the AWG is used to modulate a built-in external cavity laser of the ThorLabs MX40G 40 GHz modulator. This represents a radio over fiber transmitter system, so the output could theoretically propagate thousands of kilometers before conversion to an electrical signal. A Picometrix PT40-A photodetector performs optical to electrical conversion. It produces two electrical signals at the desired mm-Wave bands for simultaneous operation at both frequencies (24 GHz and 39 GHz). The photodetector requires two-stage amplification before input to the Rotman lens: one built-in transimpedance amplifier (TIA) and then an external power amplifier. However, high-power mmW photodetectors are feasible. [8] has demonstrated about 20 dBm of power at 20 GHz. The total measured EIRP of the transmitting dual-band Rotman lens antenna system is approximately 11 dBm at 24 GHz and 39 GHz after the photo-detector and transimpedance amplifier output (−17 dBm), power amplifier (30 dB), the minimum realized gain of the Rotman lens antenna system (8 dB) and cable losses (−10 dB).

The receiver is a horn antenna with 20 dBi of gain, located 1 m away from the transmitter. The signal received by the horn antenna is amplified with a 40 dB low-noise amplifier (LNA). This received signal is then down mixed to base band, using a passive mixer. Lastly, this output goes through a 1.5 GHz low pass filter to remove interference by higher frequency components and then it is led to the oscilloscope to analyze the eye diagrams of the received signal. Note there is no phase locked loop so the voltage of the eye varies as phase varies. With a phase locked loop (PLL) typical in homodyne receivers, more stable eye diagrams are achievable.

Before observing the oscilloscope data, the output of the horn (after amplification by the LNA) is fed into a spectrum analyzer to verify that the modulated signals are being effectively transmitted by the Rotman lens antenna and received by the horn at both operating frequencies. Two different transmit configurations are investigated: feeding a single beam port of the dual-band Rotman lens antenna (beam port 4 - single beam around 0°) and feeding multiple beam ports of the dual-band Rotman lens antenna (beam port 4 and 6 - 2 beams around 0° and 30°). All configurations transmit both 24 GHz and 39 GHz signals simultaneously. Fig. 7 shows the signal spectrum at both (a) 24 GHz and (b) 39 Hz, in the first configuration, where only beam port 4 is fed. A signal-to-noise ratio (SNR) of at least 30 dB is demonstrated at both frequencies. The bandwidth of the modulated signal is 930 MHz. Similar behaviour is demonstrated in the second configuration which demonstrates 2 simultaneous beams (multi-beam at-a-time operation), where regardless of the beam port chosen or frequency investigated, the signal to noise ratio is approximately 30 dB, and bandwidth is 930 MHz. Given the SNR ratio of 30 dB for an EIRP of 11 dBm and assuming the same receiver sensitivity, an estimated maximum communication range of 1.6 km at 24 GHz and 1.0 km at 39 GHz is expected with the maximum permissible EIRP for 5G/mmW systems, $75\,\mathrm{dBm}$. Based on Shannon's channel capacity defined as $C = Blog_2(1+S/N)$, where C is capacity, B is the bandwidth of the channel, and S/N is the SNR in linear scale, the maximum throughput we can receive with this system is $9.27\,\mathrm{Gbps}$.

The same two configurations (feeding a single beam port of the dual-band Rotman lens antenna (beam port 4) and feeding multiple beam ports of the dual-band Rotman lens antenna (beam ports 4 and 6)) are investigated using the oscilloscope. The open eyes shown in Fig. 9 (feeding through a single port), and in Fig. 10 (feeding through multiple ports at a time), show that the system performed as desired and the data received at the horn antenna is distinguishable. Each eye diagram corresponds to a continuous 4500 symbol capture on an oscilloscope. All captures are error free after counting bit errors using the encoded PRBS7 pattern. Therefore, directly measured bit error rates fall below the hard FEC threshold. Extrapolated semi-analytic bit error rate estimation further confirms all waveforms are below 10^{-6} BER [9].

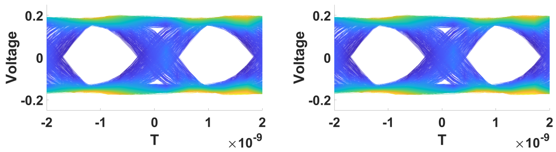

(a) (b)

Fig. 9. Eye diagrams for optically feeding beam port 4 of the dual-band Rotman lens at (a) 24 GHz and (b) 39 GHz.

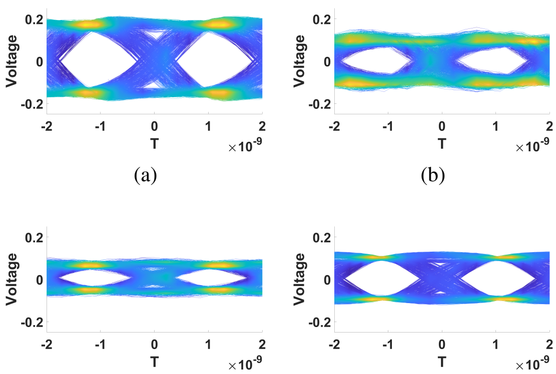

(a) (b)

(c) (d)

Fig. 10. Eye diagrams for optically feeding beam port 4 and beam port 6 of the dual-band Rotman lens to demonstrate multi-beam at a time interrogating at first beam peak (0°) at (b) 24 GHz and (b) 39 GHz and interrogating at the second beam peak (30°) at the (c) 24 GHz and (d) 39 GHz.

IV. Conclusion

A compact, low-power, dual-band, multi-beam at-a-time Rotman lens antenna array design paired with optical modulation through the use of a photodetector is presented for the application of simplifying 5G/mmW base station designs potentially enabling real-world network densification. This converged optical/mmW system greatly reduces the need for multiple individual antenna array systems, while the modulation of the data in the optical domain allows for the relocation of processing to the base station to the hub/central office location, taking of advantage of the existing fiber network in place. Additionally, through the use of higher order modulation and additional RF amplifiers, data rates on the order of several Gbps are envisioned.

References

[1] L. H. Ye, X. Y. Zhang, Y. Gao, and Q. Xue, "Wideband dual-polarized two-beam antenna array with low sidelobe and grating-lobe levels for base-station applications," *IEEE Transactions on Antennas and Propagation*, vol. 67, no. 8, pp. 5334–5343, 2019.

[2] H. Zhu, H. Sun, B. Jones, C. Ding, and Y. J. Guo, "Wideband dual-polarized multiple beam-forming antenna arrays," *IEEE Transactions on Antennas and Propagation*, vol. 67, no. 3, pp. 1590–1604, 2019.

[3] W. Rotman and R. Turner, "Wide-angle microwave lens for line source applications," *IEEE Transactions on Antennas and Propagation*, vol. 11, no. 6, pp. 623–632, 1963.

[4] M. Nikkhah, M. Hiranandani, and A. Kishk, "Rotman lens design with wideband dra array," *Progress In Electromagnetics Research*, vol. 169, pp. 45–57, 01 2020.

[5] A. Darvazehban, O. Manoochehri, M. A. Salari, P. Dehkhoda, and A. Tavakoli, "Ultra-wideband scanning antenna array with rotman lens," *IEEE Transactions on Microwave Theory and Techniques*, vol. 65, no. 9, pp. 3435–3442, 2017.

[6] C. A. Lynch, A. O. Adeyeye, A. Eid, J. Hester, and M. M. Tentzeris, "Ultra-long-range dual rotman lenses-based harmonic mmld's for 5g/mm-wave lot applications," in *2022 IEEE/MTT-S International Microwave Symposium - IMS 2022*, 2022, pp. 32–35.

[7] A. Eid, J. Hester, and M. M. Tentzeris, "Optimizing rotmen lens topologies for 5g wireless grids," in *2021 IEEE International Symposium on Antennas and Propagation and USNC-URSI Radio Science Meeting (APS/URSI)*, 2021, pp. 1061–1062.

[8] Z. Li, Y. Fu, M. Piels, H. Pan, A. Beling, J. E. Bowers, and J. C. Campbell, "High-power high-linearity flip-chip bonded modified uni-traveling carrier photodiode," *Opt. Express*, pp. B385–B390, 2011.

[9] G. P. Agrawal, "Fiber-optic communication systems," 2010.